Applied Physics Letters

Surface and size effects on phase diagrams of ferroelectric thin films

Cite as: Appl. Phys. Lett. **95**, 262901 (2009); https://doi.org/10.1063/1.3272942
Submitted: 02 September 2009 . Accepted: 12 November 2009 . Published Online: 28 December 2009

D. C. Ma, Yue Zheng, and C. H. Woo

Surface and size effects on phase diagrams of ferroelectric thin films

D. C. Ma, Yue Zheng,[a] and C. H. Woo[b]
Department of Electronic and Information Engineering, The Hong Kong Polytechnic University, Hong Kong SAR, Hong Kong

(Received 2 September 2009; accepted 12 November 2009; published online 28 December 2009)

Taking into account effects of the surface and depolarization field, we investigated the "misfit strain-temperature" phase diagrams of ferroelectric thin film by using the time-dependent Ginzburg–Landau theory. The simulation results show that the surface effect can shift the phase diagram to lower temperature. More importantly, effect of the depolarization field obviously shrinks the *c*-phase, and dominates the paraelectric and *aa*-phase in the phase diagram. © *2009 American Institute of Physics*. [doi:10.1063/1.3272942]

Due to the surface, depolarization field or size effects, it is well known that the physical properties of ferroelectric thin film (FTF) significantly differ from those of bulk ferroelectrics.[1–10] Theoretically, Ginzburg–Landau (GL) phenomenological theory has been developed to describe the surface and size effects of FTF. In this theory, some coefficients of the free energy expansion, such as the Curie temperature, can be modified to be size dependent. The so-called extrapolation length is introduced to describe the difference of the spontaneous polarization between the surface and the interior of ferroelectric materials.[4–10]

When a FTF epitaxially grows on cubic substrates, the mechanical constraints also affect its phase transition characteristics.[11–16] So the "misfit strain-temperature" (MST) phase diagrams are very important for designing miniature electric device. The initial versions of MST phase diagrams were plotted using thermodynamic analyses with a single, homogeneous domain state.[11] Subsequently, taking into account the three dimensional domain structures, Pertsev *et al.*[12] has given the phase diagram based on a model of the modified Gibbs free energy, and Chen *et al.*[13,14] developed the phase diagrams by using the time-dependent Ginzburg–Landau (TDGL) equations. However, these models were based on a hypothesis that the film thickness is greater than the ferroelectric correlation length, i.e., $h > 50$ nm. For a FTF, i.e., $h \ll 50$ nm, the surface and depolarization field effects have to be considered when we investigate the phase diagrams. Using GL approach, Morozovska *et al.*[15] considered effects of the surface, misfit strain, and size effects, approximately and analytically given the phase diagrams of epitaxial FTF (i.e., using finite extrapolation length). Up to now, rigorous results of the MST phase diagrams have not been obtained with considering effects of the surface and depolarization field. In this letter, we developed a phase field model (PFM) based on TDGL to predict the MST phase diagrams as functions of the FTF thickness. Due to effects of the surface and depolarization field, the phase diagrams can be shifted obviously with changing the film thickness.

It is known that the spontaneous polarization occurs in a ferroelectric material when the temperature is lower than its Curie point, thereby leading to the paraelectric-to-ferroelectric phase transition. At constant stress and temperature, the total polarization field $\mathbf{P}^{\mathrm{T}}$ can be divided into two components, the spontaneous polarization $\mathbf{P}$ and induced polarization $\mathbf{P}^{\mathrm{E}}$ which is assumed to be linearly proportional to the electric field, i.e., $\mathbf{P}^{\mathrm{E}}=\boldsymbol{\chi}_{\mathbf{b}}\mathbf{E}$, where $\boldsymbol{\chi}_{\mathbf{b}}$ are the background dielectric susceptibilities.[7–10,17–19] The electric displacement field $\mathbf{D}$ can be in terms of the spontaneous polarization as,

$$\mathbf{D} = \varepsilon_0\mathbf{E} + \mathbf{P}^{\mathbf{T}} = \varepsilon_0\mathbf{E} + \mathbf{P}^{\mathbf{E}} + \mathbf{P} = \varepsilon_0\mathbf{E} + \boldsymbol{\chi}_{\mathbf{b}}\mathbf{E} + \mathbf{P} = \boldsymbol{\varepsilon}_{\mathbf{b}}\mathbf{E} + \mathbf{P}, \tag{1}$$

where ε_0 and $\boldsymbol{\varepsilon}_{\mathbf{b}}$ are the dielectric constants of the vacuum and background material, respectively.[14–16,18–23]

The local spontaneous polarization vector, $\mathbf{P}(\mathbf{x}) = [P_1, P_2, P_3]$, are taken as the order parameter of the Landau-type free energy, where $\mathbf{x}=(x_1, x_2, x_3)$. The temporal evolution of the polarization is calculated from the following TDGL equation as,

$$\frac{\partial \mathbf{P}(\mathbf{x},t)}{\partial t} = -M\frac{\delta F}{\delta \mathbf{P}(\mathbf{x},t)}, \tag{2}$$

where M is a kinetic coefficient, t is time, F is the total free energy of the system.

According to previous works,[11–22] the total free energy can be expressed as,

$$\begin{aligned} F &= F_0 + F_{\mathrm{bulk}} + F_{\mathrm{grad}} + F_{\mathrm{elas}} + F_{\mathrm{surf}} + F_{\mathrm{elec}} \\ &= F_0 + \int\int\int_V [f_{\mathrm{bulk}} + f_{\mathrm{elas}} + f_{\mathrm{grad}} + f_{\mathrm{elec}}]dV + \int\int_S f_{\mathrm{surf}}dS, \end{aligned} \tag{3}$$

where F_0, F_{bulk}, F_{grad}, F_{elas}, F_{surf}, and F_{elec} are the polarization-independent, bulk-free, gradient, elastic strain, surface, and electric energies, respectively. V is the volume of the thin film. S is the upper-lower surface of FTF.

The bulk free energy density f_{bulk} can be expressed by the Landau polynomial expansion in terms of the polarization components,[5]

$$\begin{aligned} f_{\mathrm{bulk}} = {} & \alpha_1(P_1^2 + P_2^2 + P_3^2) + \alpha_{11}(P_1^4 + P_2^4 + P_3^4) + \alpha_{12}(P_1^2P_2^2 \\ & + P_2^2P_3^2 + P_1^2P_3^2) + \alpha_{111}(P_1^6 + P_2^6 + P_3^6) + \alpha_{112}[P_1^4(P_2^2 \\ & + P_3^2) + P_2^4(P_1^2 + P_3^2) + P_3^4(P_1^2 + P_2^2)] + \alpha_{123}P_1^2P_2^2P_3^2, \end{aligned} \tag{4}$$

where $\alpha_1=(T-T_0)/2\varepsilon_0C_0$ is the dielectric stiffness, and C_0

[a]Also at: School of Physics and Engineering, Sun Yat-Sen University, GuangZhou, China. Electronic mail: zhengy35@mail.sysu.edu.cn.
[b]Electronic mail: chung.woo@polyu.edu.hk.

and T_0 are the Curie constant and Curie–Weiss temperature of the reference crystals, respectively. α_{11}, α_{12}, α_{111}, α_{112}, and α_{123} are higher order dielectric stiffnesses.

In Eq. (3), f_{grad} is the gradient energy density, and can be calculated through the gradients of the polarization field,

$$f_{\text{grad}} = \tfrac{1}{2} g_{ijkl} P_{i,j} P_{k,l}, \tag{5}$$

where $\partial P_i / \partial x_j$ are expressed by $P_{i,j}$, and g_{ijkl} are the gradient energy coefficients.

The elastic energy density f_{elas} is generated from the phase transition and the substrate constraint, and can be generally given by,

$$f_{\text{elas}} = \tfrac{1}{2} c_{ijkl} (\varepsilon_{ij} - \varepsilon_{ij}^0)(\varepsilon_{kl} - \varepsilon_{kl}^0), \tag{6}$$

where c_{ijkl} is the elastic stiffness tensor, ε_{ij} and ε_{ij}^0 are the total strain and eigenstrain, respectively. The eigenstrain connected with the ferroelectric transition is $\varepsilon_{ij}^0 = Q_{ijkl} P_k P_l$, in which Q_{ijkl} represent the electrostrictive coefficients.

Due to the surface effect, the spontaneous polarizations are inhomogeneous across the out-of-plane direction of FTF. Therefore, this intrinsic phenomenon is taken into account through the surface energy density f_{surf}, which can be approximately characterized by the effective extrapolation length δ_i^{eff},[5]

$$f_{\text{surf}} = \frac{D_{11} P_1^2}{2\delta_1^{eff}} + \frac{D_{22} P_2^2}{2\delta_2^{eff}} + \frac{D_{44} P_3^2}{2\delta_3^{eff}}, \tag{7}$$

where D_{11}, D_{22}, and D_{44} are material coefficients from gradient energy coefficients.

Generally speaking, the depolarization field for the short-circuit boundary conditions has two contributions, one coming from the incomplete charge compensation in the electrodes, and the other due to the inhomogeneous polarization field near the surface. In this work, we only consider that the electrodes are perfect metals, and the depolarization filed is only induced by inhomogeneous spontaneous polarization. In absence of the external electric field, the electric energy density is only determined by the depolarization field, i.e., $\mathbf{E}=\mathbf{E}_{\text{d}}$. In the case of our work, $\mathbf{E}_{\text{d}}$ is mainly determined by the spontaneous polarization along normal orientation of the FTF surface, and can be given by $E_{\text{d}} = -\varepsilon_b^{-1}(P_3 - \langle P_3 \rangle) = -\varepsilon_b^{-1}(P_3 - \frac{1}{h}\int_0^h P_3 dx_3)$.[19,20] The depolarization energy density of Eq. (3) can be expressed as,

$$f_{\text{elec}} = f_{\text{dep}} = \frac{1}{2\varepsilon_b}[P_3^2(x_3) - \langle P_3 \rangle^2]. \tag{8}$$

In the simulations, we employ $64 \times 64 \times N$ discrete grid points at a scale of $\Delta x_1 = \Delta x_2 = 1$ nm and $\Delta x_3 = 0.2$ nm to model $PbTiO_3$ thin film grown on $SrTiO_3$ substrate with the short-circuit boundary conditions. Parameters in calculations are listed in Ref. 24, which were taken from Refs. 5, 12, 25, and 26. The film thicknesses are represented by the letter N in the x_3 direction. Periodic boundary conditions are employed along the x_1 and x_2 directions. The MST phase diagrams were generated by assuming a single domain state in FTF.

According to previous works,[12] we know that the MST phase diagrams have the p-phase ($P_1=P_2=P_3=0$), c-phase ($P_1=P_2=0$, $P_3\neq 0$), aa-phase ($P_1=P_2\neq 0$, $P_3=0$), and r-phase ($P_1=P_2\neq 0$, $P_3\neq 0$), respectively. It is well-known that positive misfit strain (i.e., tensile stress) favors the appearance of the aa-phase, while the negative misfit strain (i.e., compressive stress) induces the c-phase. In this letter,

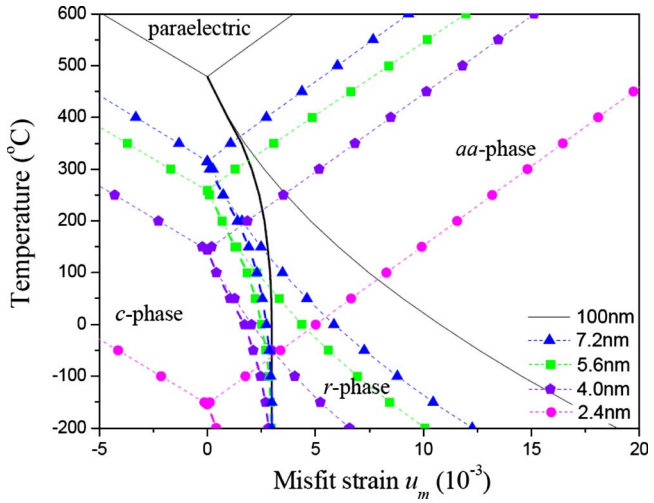

FIG. 1. (Color online) Misfit strain-temperature phase diagrams of the $PbTiO_3$ film with different thickness under the surface and size effects: Solid lines are a reference state comparing with Ref. 12, and scattered symbols are phase boundaries from phase field simulation separating c-, r-, aa-, and p-phase regions. The first and second order phase transitions are shown by thick and thin lines, respectively.

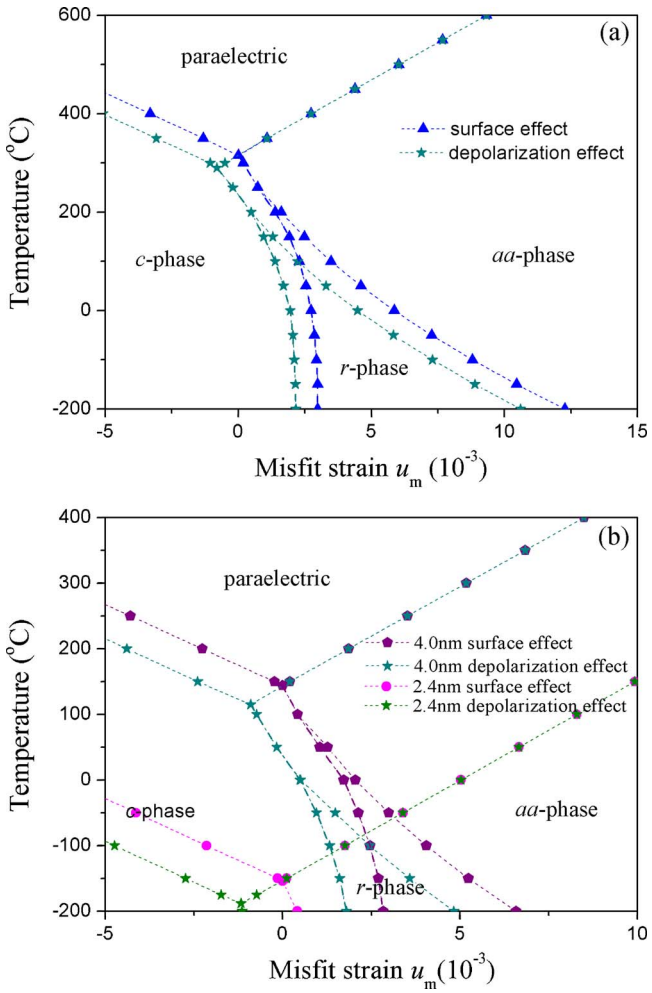

FIG. 2. (Color online) The influence of depolarization effects on MST phase diagram with different film thicknesses (a) 7.2 nm, (b) 4.0 nm and 2.4 nm. Scattered symbols are phase boundaries from the phase field simulation separating c-, r-, aa-, and p-phase regions. The first and second order phase transitions are shown by thick and thin lines, respectively.

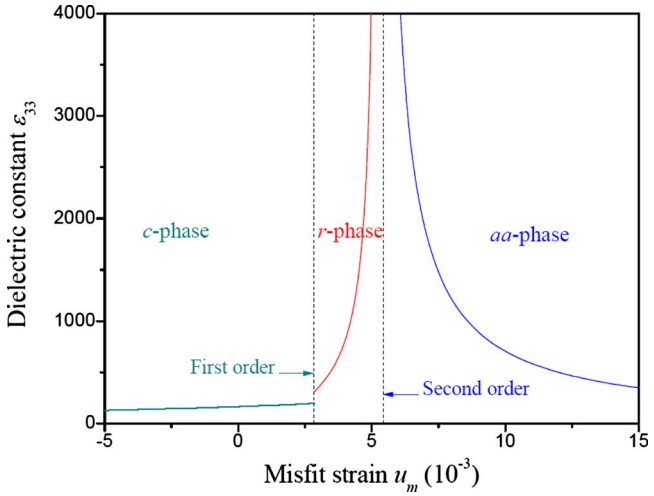

FIG. 3. (Color online) The dependence of the dielectric constant ε_{33} of $PbTiO_3$ films on misfit strain u_m with film thickness 7.2 nm at room temperature.

the $PbTiO_3$ thin films with thicknesses of 2.4, 4.0, 5.6, and 7.2 nm are first considered to show the influence of surface effect on MST diagrams. Based on numerical simulations, we plot the phase diagrams as functions of the film thickness are shown in Fig. 1. It is noted that, for presenting the surface effect, we first neglect effect of the depolarization effect on the MST diagrams. In Fig. 1, solid line give the MST phase diagram of FTF with a very large thickness, i.e., $h=100$ nm. At a given misfit strain, the phase transition temperature of the *aa*-phase and *c*-phase, where the transition from paraelectric state to *c* or *aa* ferroelectric phases occurs, is shifted as a result of the surface effect. Results show that the surface effect can lead to a decrease in the phase transition temperature. With the film thickness decreasing, the *c*-phase, *aa*-phase, and *r*-phase shrink, and *p*-phase dominates.

When the electric energy determined by the depolarization field is incorporated into the total free energy Eq. (3), we can develop the MST phase diagram as shown in Fig. 2. It is known that the depolarization field induced by the polarization component perpendicular to the plane of thin film P_3 will reduce the magnitude of polarization P_3. When the film thickness is sufficiently reduced, the inhomogeneous polarization along x_3 direction will enhance the depolarization field. Simultaneously, the Curie temperatures corresponding to the polarization P_3 descend with the film thickness. Figure 2 also show that the influence of depolarization field on phase diagram is different with that in Fig. 1 due to the surface effect. The depolarization field effect only shifts the diagram as a whole along the line between *p*-phase and *aa*-phase, these results are also similar to results of the phase diagram about the ferroelectric superlattices.[27]

The influence of the misfit strain on the dielectric response ε_{33} is shown in Fig. 3. It can be seen that two jumps of ε_{33} happen at the *c*-phase/*r*-phase transition and the *r*-phase/*aa*-phase transition. The first jump of ε_{33} corresponds to *c*-phase/*r* phase transition in which is the first order phase transition. The sudden appearance or disappearance of the polarization P_1 and P_2 result in the jump of ε_{33} curve. Similarly, the other jump of ε_{33} corresponds to *r*-phase/*aa*-phase transition that is of the second order. The disappearance or appearance of P_3 brings about the jump of ε_{33} curve.

In summary, we have described a PFM to simulate the MST phase diagram of FTF with the surface and depolarization effects. The results show that it is possible to reach the phase-transition conditions by changing the thickness of FTF. Accordingly, FTF thickness can be chosen as design parameters to manipulate the Curie temperature thus making them attractive for various microelectronic applications.

This project was supported by grants from RGC of HKSAR (Grant Nos. G-YX0T, 5322/04E, and N53408). Y.Z. is also grateful for support from NSFC (Grant Nos. 10902128 and 10831160504).

[1] A. N. Morozovska, S. V. Kalinin, E. A. Eliseev, V. Gopalan, and S. V. Svechnikov, Phys. Rev. B **78**, 125407 (2008).
[2] K. Binder, Ferroelectrics **35**, 99 (1981).
[3] M. Q. Cai, Y. J. Zhang, Z. Yin, and M. S. Zhang, Phys. Rev. B **72**, 075406 (2005).
[4] Y. Zheng, C. H. Woo, and B. Wang, J. Phys.: Condens. Matter **20**, 135216 (2008).
[5] L. Hong, A. K. Soh, Y. C. Song, and L. C. Lim, Acta Mater. **56**, 2966 (2008).
[6] Y. L. Li, S. Y. Hu, D. Tenne, A. Soukiassian, D. G. Schlom, and X. X. Xi, Appl. Phys. Lett. **91**, 112914 (2007).
[7] Y. Zheng, C. H. Woo, and B. Wang, Nano Lett. **8**, 3131 (2008).
[8] Y. Zheng, B. Wang, and C. H. Woo, Acta Mater. **56**, 479 (2008).
[9] B. Wang and C. H. Woo, J. Appl. Phys. **97**, 084109 (2005).
[10] Y. Zheng, B. Wang, and C. H. Woo, Phys. Lett. A **368**, 117 (2007).
[11] R. S. Beach, J. A. Borchers, A. Matheny, R. W. Erwin, M. B. Salamon, B. Everitt, K. Pettit, J. J. Rhyne, and C. P. Flynn, Phys. Rev. Lett. **70**, 3502 (1993).
[12] N. A. Pertsev, A. G. Zembilgotov, and A. K. Tagantsev, Phys. Rev. Lett. **80**, 1988 (1998).
[13] N. A. Pertsev and V. G. Koukhar, Phys. Rev. Lett. **84**, 3722 (2000).
[14] Y. L. Li, S. Y. Hu, Z. K. Liu, and L. Q. Chen, Appl. Phys. Lett. **78**, 3878 (2001).
[15] M. D. Glinchuk, A. N. Morozovska, and E. A. Eliseev, J. Appl. Phys. **99**, 114102 (2006).
[16] Y. L. Li and L. Q. Chen, Appl. Phys. Lett. **88**, 072905 (2006).
[17] B. Wang and C. H. Woo, J. Appl. Phys. **100**, 044114 (2006).
[18] Y. Zheng and C. H. Woo, Nanotechnology **20**, 075401 (2009).
[19] C. H. Woo and Y. Zheng, Appl. Phys. A: Mater. Sci. Process. **91**, 59 (2008).
[20] Y. Zheng and C. H. Woo, Appl. Phys. A: Mater. Sci. Process. **97**, 617 (2009).
[21] M. E. Lines and A. M. Glass, *Principles and Applications of Ferroelectrics and Related Materials* (Clarendon, Oxford, 1979).
[22] C. Kittel, *Introduction to Solid State Physics* (Wiley, New York, 2005).
[23] D. C. Lupascu, *Fatigue in Ferroelectric Ceramics and Related Issues* (Springer, Berlin, 2004).
[24] Parameters used in the calculations are $\alpha_1=3.8\times(T-752)\times10^5$, $\alpha_{11}=-7.3\times10^7$, $\alpha_{12}=7.5\times10^8$, $\alpha_{111}=2.6\times10^8$, $\alpha_{112}=6.1\times10^8$, $\alpha_{123}=-3.7\times10^9$, $Q_{11}=0.089$, $Q_{12}=-0.026$, $Q_{44}=0.03375$, $s_{11}=8.0\times10^{-12}$, $s_{12}=-2.7\times10^{-12}$, $s_{44}=9.24\times10^{-12}$, $\delta_1^{eff}=\delta_2^{eff}=\delta_3^{eff}\approx2.8$ nm, and $\varepsilon_b\approx50\varepsilon_0$.
[25] L. Q. Chen, *Physics of Ferroelectrics* (Springer, Berlin, 2007), Vol. 105, p. 363.
[26] J. Zhang, Z. H. Wu, Z. Yin, and M. S. Zhang, Integr. Ferroelectr. **43**, 19 (2002).
[27] F. A. Urtiev, V. G. Kukhar, and N. A. Pertsev, Appl. Phys. Lett. **90**, 252910 (2007).